# Modeling and analysis of propulsion in the multiflagellated micoorganism *Giardia lamblia*

Scott C. Lenaghan,* Jun Chen,* and Mingjun Zhang†
*Department of Mechanical, Aerospace, and Biomedical Engineering, University of Tennessee, Knoxville, Tennessee 37996, USA*
(Received 13 March 2013; revised manuscript received 16 May 2013; published 29 July 2013)

The goal of this work was to analyze the propulsion of multiflagellated microorganisms, and to draw insight to the underlying physics and biology of the movement. *Giardia lamblia* was chosen as the model organism due to its unique ability to mechanically attach to various surfaces, its rapid movement, and its fine control over steering and navigation. In this work, a mechanics model was utilized to study the mechanics and propulsive contribution of the ventral and anterior flagella in *Giardia*. It was discovered that energy is supplied mainly at the proximal portion of these flagella, supporting the hypothesis that a decreasing adenosine triphosphate (ATP) gradient along the length of the flagella would not affect the motion observed. Similarly, the elasticity of the flagella allows the energy input at the proximal portion to be transferred to the distal portion, where the majority of thrust is generated. Specifically, we found that the ventral flagella are the driving force for planar propulsion and turning, while the anterior flagella are used for steering and control.

DOI: 10.1103/PhysRevE.88.012726 PACS number(s): 87.17.Jj, 87.85.gf, 87.85.St

## I. INTRODUCTION

The rapidly emerging need for site-specific controlled drug delivery, along with the development of less invasive surgical procedures, has necessitated the development of swimming microrobots [1–4]. Ideally, these robots should be able to maneuver through complex biological environments, including blood vessels, and both the gastrointestinal and urinary tracts. Microrobots have even been envisioned to navigate through the ureter to break up kidney stones [5] and deliver drugs to specific sites after injection [6]. Despite the broad range of applications for microrobots, a key obstacle remains in the design of swimming microrobots capable of propulsion at low Reynold's numbers ($10^{-5}$–$10^{-4}$) [7]. In this microenvironment, simple reciprocal motion, similar to a scallop, will not result in a propulsive force and thus zero net movement. To counteract this problem, microorganisms have developed unique structures, cilia and flagella, to generate nonreciprocal traveling waves to achieve a net forward motion [7–9]. Both of these flexible filamentous structures are capable of generating a bending moment that can be translated into propulsion [10]. This bending moment is mechanically generated by the sliding of microtubules, and is actuated by motor proteins bound to the microtubules [11,12]. In the case of prokaryotic flagella, a helical wave form is generated that acts as a rotary propeller to move the organism [13]. Eukaryotic flagella, however, function by generating a planar wave form that drives them forward [13]. The highly conserved nature of these structures indicates that they are ideally suited for microscale propulsion, and thus serve as a key source for bioinspired microrobot design [14]. Considering the importance of understanding the propulsion of different microorganisms, we have chosen to examine swimming and propulsion of a multiflagellated eukaryotic parasite, *Giardia lamblia*.

*Giardia lamblia* has several key features that make it attractive for the study of micropropulsion. First, the organism is a parasite of the gastrointestinal tract in a wide variety of animals including birds, reptiles, mammals, and fish [15–20]. *Giardia*'s natural habitat, the mammalian body, validates the use of its swimming mechanics for use inside the body for microsurgery or drug delivery. Second, *Giardia* has a unique attachment mechanism, which is used to attach to the intestinal epithelium. Experimentally this mechanism has been proven to be highly robust, allowing the cells to attach to glass, plastic, and many other surfaces, regardless of surface properties [21–25]. This rapid mechanical attachment to tissue could play an important role in site-specific drug delivery, and understanding this mechanism may lead to the development of more efficient *in vivo* attachment microdevices. Third, the motile stage of *Giardia* is shaped like an airfoil, which may represent an ideal shape for the cell body, unlike the ellipsoidal body of sperm and bacteria. Fourth, *Giardia* is able to rapidly form a monolayer on a surface, both *in vivo* and *in vitro*, indicating fine control over their movement [26]. Despite the presence of thousands to millions of cells, *Giardia* can still closely align themselves with one another, leaving a minimal amount of space between neighboring cells. Finally, *Giardia* uses a complex and unique arrangement of cytoskeletal components to swim. Whereas traditional flagella exit the cytoplasm at the rear of the cell, the various flagella in *Giardia* exit at different locations along the body, indicating multiple functions for different pairs of flagella. As shown in Fig. 1, the four pairs of flagella in *Giardia* have distinct positions along the body wall. Two pairs of flagella, the anterior (black, 1) and posterolateral (red, 2), exit the cytoplasm symmetrically at the sides of the body. The caudal flagella (blue, 4) exit at the caudal apex, and extend behind the cell. The ventral flagella (yellow, 3) emerge from behind the adhesive disc and are bounded by the ventrocaudal groove. Interestingly, the flagella are all anchored at nearly the same point inside of the cell, and all have significant cytoplasmic portions (dotted lines). While the anterior, posterolateral, and caudal flagella are cylindrical, the ventral flagella have a ventral-facing fin that

*These authors equally contributed to this work.

†Corresponding author: Mingjun Zhang, Department of Mechanical, Aerospace, and Biomedical Engineering, University of Tennessee, 1512 Middle Drive, 408 Dougherty Hall, Knoxville, TN 37996. Email address: mjzhang@utk.edu

 

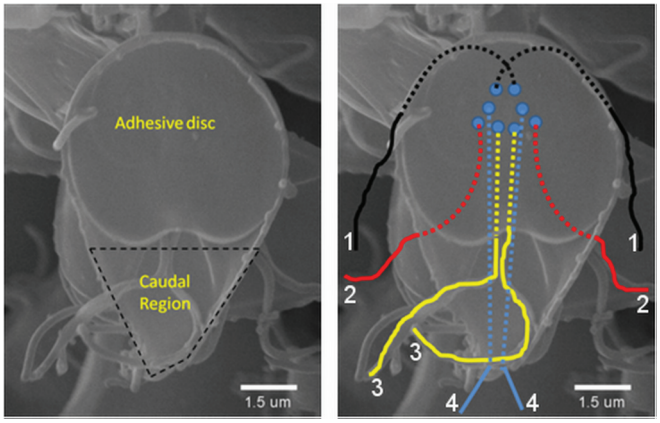


FIG. 1. (Color online) Ventral morphology of *Giardia*. The circular adhesive disc makes up the anterior region of the cell, while the caudal region lacks this rigid cytoskeleton. Dotted lines indicate cytoplasmic components of the flagella. Solid lines indicate portions of flagella able to move outside of the cell.

runs the length of the flagella. The modification of this flagella pair has a significant effect on the fluid motion generated by these flagella [27,28]. Recent studies have demonstrated that multiflagellated organisms often have different optimal propulsive wave forms when compared to single posterior flagellated organisms, necessitating the need for further study [29].

In a previous study, we experimentally analyzed the flagella motion of *Giardia* [Figs. 2(a) and 2(b)] using an advanced imaging platform [26]. It was discovered that *Giardia* is capable of three-dimensional swimming of 20–40 $\mu$m/s through undulation of the caudal region of the body, and slower planar motion (1–15 $\mu$m/s), where the propulsive force is generated from the motion of the flagella. During the planar motion, the cell has precise directional control and maintains a stable orientation through manipulation of the multiple flagella pairs. This movement is crucial to the rapid formation of a nearly complete monolayer during infection. In 2012, we developed a dynamics model for the swimming of *Giardia* based on resistive force theory (RFT) [30]. Using this model we conducted simulations to identify the contribution of the cilialike beating of the anterior and posterolateral flagella to both forward propulsion and turning. It was discovered that it was only necessary to supply power to the proximal portion of these flagella, and that energy would be passively transferred along the length of the flagella [30]. It was also discovered that the propulsive efficiency through the use of only the anterior and posterolateral flagella was half that of sperm. This was hypothesized to be due to the backward motion of the body during the upstroke of these flagella, which has not been observed experimentally [26]. The conclusions from this study led to the hypothesis that the ventral flagella were a key driving force for efficient forward propulsion. In addition, while this model was able to obtain quantitative data for the ciliary beating of the anterior and posterolateral flagella, the implications of these data on the biology and physics of *Giardia* movement was not analyzed.

In this study we have expanded on our earlier work making several contributions to the study of multiflagellated propulsion in *Giardia*: (1) Kinematic data for the beating of the ventral and anterior flagella were obtained using the previously developed microscopic platform. (2) The previously developed analytical mechanics model of flagella-body-fluid interactions was modified to analyze the effect of the ventral flagella on forward swimming, and test the hypothesis that the ventral flagella prevent the backward motion observed with the beating of only the anterior and posterolateral flagella [30]. (3) The bending moments obtained from the analytical model were used to calculate the dynein motor forces in *Giardia*, and these forces were compared to the results obtained from previous studies. (4) The required actuation bending moment, as well as the energy input used by *Giardia* to achieve the observed planar swimming motion, was predicted. Based on these data, it was possible to compare previous hypotheses on the transport of adenosine triphosphate (ATP) to the flagella compartment, and identify the most likely mechanism of transport in *Giardia*. Few studies have been conducted to understand the actuation pattern along a flagellum and the associated mechanical energy supply; however, this information will aid in understanding propulsion in microorganisms. (5) Thrust along the ventral and anterior flagella was calculated from the model, and used to determine the contribution of each of these flagella pairs to propulsion and turning. (6) Finally, the results obtained from the experimental and modeling analysis were discussed in terms of bioinspiration for micropropulsive system design for future generations of microrobots.

## II. MODEL OF FLAGELLA-BODY-FLUID INTERACTION DYNAMICS

In a previous study, the flagella and cell body of *Giardia* were modeled as a multibody system [30]. In this model, a nondeformable body form was used [26] and the mechanics of the flagella were modeled as a chain of rigid links [31,32]. The fluid forces in the model were represented as a static function of relative velocity between the flagella or body and the fluid (i.e., resistive force theory) [33,34]. In this work, predictions on the actuation bending moment applied along the anterior and ventral flagella and the thrust distribution were obtained through simulation of the analytical flagella-body-fluid interaction model described below. Additional equations and derivation of the model can be found in [30].

### A. Body model

The flagella-body system was decomposed into body and flagella subsystems. The cell body was approximated as a rigid sphere, whose translational ($c_l^b$) and rotational ($c_o^b$) drag coefficients are given by [35]

$$c_l^b = 6\pi\mu a, \quad c_o^b = 8\pi\mu a^3,$$

where $a$ is the radius of the body. Our analysis indicated that the characteristics of thrust distribution, actuation bending moment, and energy supply and dissipation along the flagellum predicted by the model were insensitive to the swimming speed of the microorganism. Thus this approximation of the cell body as a sphere did not prevent us from obtaining the propulsive characteristics of *Giardia*.

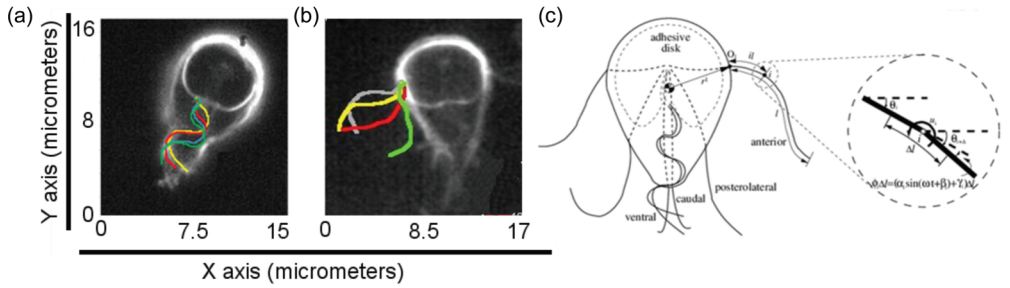


FIG. 2. (Color online) Characteristic flagella traces and schematic of the flagella model for *Giardia*. (a) and (b) Experimental images of *Giardia* and plots of typical ventral (a) and anterior (b) flagella traces over time. The swimming episodes were carefully chosen so that the ventral or anterior flagellum remained in focus for the entire beating cycle. The beat duration of the anterior and ventral flagella was ∼60 and ∼72 ms, respectively. (c) Diagram of the cytoskeleton of *Giardia* indicating the flagella pairs. In addition, a schematic of the flagella model is displayed in the expanded view.

At low Reynold's number, inertial effects are neglected; thus the force balance on the cell body is generated from the fluid force (torque) and the reaction forces (torques) from the multiple flagella at their point of exit from the body. The reaction forces at the exit locations induce additional torque with respect to the geometry center of the body. The equations for the motion of the cell body are shown below [30]:

$$s\begin{bmatrix} -c_l^b & 0 \\ 0 & -c_l^b \end{bmatrix} s^{\mathrm{T}}\begin{bmatrix} \dot{z}_x \\ \dot{z}_y \end{bmatrix} + \begin{bmatrix} \sum_{k=1}^{p} h_{x_1}^k \\ \sum_{k=1}^{p} h_{y_1}^k \end{bmatrix} = 0,$$

$$-c_o^b\dot{\theta}^b + \sum_{k=1}^{p}\begin{bmatrix} -r_y^k & r_x^k \end{bmatrix} s^{\mathrm{T}}\begin{bmatrix} h_{x_1}^k \\ h_{y_1}^k \end{bmatrix} + \sum_{k=1}^{p} u_1^k = 0,$$

where $\dot{z}_x$, $\dot{z}_y$, and $\dot{\theta}^b$ are the translational and angular velocities of the geometry center of the body in the inertial frame of reference. $h_{x_1}^k$, $h_{y_1}^k$, and $u_1^k$ are the forces and bending moment exerted on the cell body by the $k$th flagellum. $[r_x^k r_y^k]^{\mathrm{T}}$ are the locations where the flagella exit the body in the body frame of reference, while $s := \begin{bmatrix} \cos\theta^b & -\sin\theta^b \\ \sin\theta^b & \cos\theta^b \end{bmatrix}$ is the transformation matrix between the body frame of reference and the inertial frame of reference.

### B. Flagella model

As shown in Fig. 3, the fluid forces on a segment of the flagella of length $\Delta l$ in an infinite Stokes flow are given by

$$f_t = -c_t v_t \Delta l, \quad f_n = -c_n v_n \Delta l,$$

where $v_t$ and $v_n$ are the segment velocity in the longitudinal and normal directions. $f_t$ and $f_n$ are the corresponding fluid forces on the segment [36], while $c_t$ and $c_n$ are the longitudinal and normal drag coefficients [34]:

$$c_t = \frac{2\pi\mu}{\ln(2\lambda/b) - 1/2}, \quad c_n = \frac{4\pi\mu}{\ln(2\lambda/b) + 1/2}.$$

In these equations, $\mu$ is the fluid viscosity, $b$ is the radius of the flagella, and $\lambda$ is the wavelength.

Each flagellum was modeled by a chain of rigid links connected by frictionless rotational joints with the actuation bending moments applied at the joints [Figs. 3(a) and 3(b)]. Due to the low Reynold's number, the equation of motion of each link on the flagella is a balance of fluid forces and reaction forces from adjacent links [Fig. 3(b)]:

$$f_{x_i} + h_{x_{i+1}} - h_{x_i} = 0, \tag{1}$$

$$f_{y_i} + h_{y_{i+1}} - h_{y_i} = 0, \tag{2}$$

$$u_{i+1} - u_i + (h_{y_i} + h_{y_{i+1}})l_i\cos\theta_i - (h_{x_i} + h_{x_{i+1}})l_i\sin\theta_i = 0. \tag{3}$$

$h_{x_i}$ and $h_{y_i}$ are the reaction forces from adjacent links, $u_i$ is the actuation bending moment applied at the $i$th joint, and $l_i$ is half of the link length.

By canceling the internal reaction forces $h_{x_i}$, $h_{y_i}$, we assemble an equation for $n$ links into the matrix form:

$$\begin{bmatrix} f_{x_i} \\ f_{y_i} \end{bmatrix} = \begin{bmatrix} \cos\theta_i & -\sin\theta_i \\ \sin\theta_i & \cos\theta_i \end{bmatrix}\begin{bmatrix} f_{t_i} \\ f_{n_i} \end{bmatrix}. \tag{4}$$

Noting that the fluid forces $f_{t_i}$ and $f_{n_i}$, given by Eq. (4), can further be expressed in terms of the angular velocity of the

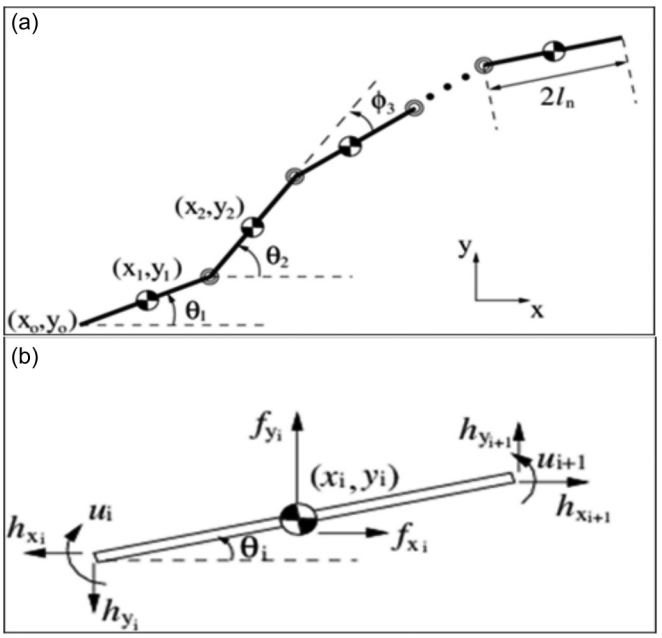


FIG. 3. Schematic representation of the flagella model. (a) Link chain model for flagellum. (b) Force diagram on the $i$th link.

links $\dot{\theta}_i$, and the translational velocity of the flagellum $\dot{x}_o$ and $\dot{y}_o$ [Fig. 3(a)], we derived the equations of motion for the $k$th flagellum, as described previously [30]:

$$\begin{bmatrix} h^k_{x_1} \\ h^k_{y_1} \end{bmatrix} = -E^{\mathrm{T}} \Omega^{\mathrm{T}}_{\theta^k} \Gamma \Omega_{\theta^k} \left( N_{\theta^k} \dot{\theta}^k + E \begin{bmatrix} \dot{x}^k_o \\ \dot{y}^k_o \end{bmatrix} \right), \tag{5}$$

$$u^k_1 = -e^{\mathrm{T}} N^{\mathrm{T}}_{\theta^k} \Omega^{\mathrm{T}}_{\theta^k} \Gamma \Omega_{\theta^k} \left( N_{\theta^k} \dot{\theta}^k + E \begin{bmatrix} \dot{x}^k_o \\ \dot{y}^k_o \end{bmatrix} \right). \tag{6}$$

In these equations, $\theta^k \in R^{n^k}$ is a column vector of link angles of the $k$th flagellum and $[x^k_o\, y^k_o]^{\mathrm{T}}$ are the positions where the flagella exit the body in the inertial frame of reference. These positions are related to the body geometry center by Eq. (7):

$$\begin{bmatrix} \dot{x}^k_o \\ \dot{y}^k_o \end{bmatrix} = \begin{bmatrix} \dot{z}_x \\ \dot{z}_y \end{bmatrix} + \dot{\theta}^b s \begin{bmatrix} -r^k_y \\ r^k_x \end{bmatrix}. \tag{7}$$

The definition of the other matrices can be found in [30]. By replacing $h^k_{x_1}$, $h^k_{y_1}$, and $u^k_1$ in the equations of motion for the cell body (Sec. II A) with Eq. (5), we get the relationship between the flagella motion and the body translational motion:

$$\sum_{k=1}^{p} G_{\theta^k} \dot{\vartheta}^k + \left( \sum_{k=1}^{p} Q_{\theta^k} + D_{\theta^b} \right) \begin{bmatrix} \dot{\theta}^b \\ \dot{z}_x \\ \dot{z}_y \end{bmatrix} = 0, \tag{8}$$

where $\dot{\vartheta}^k := \dot{\theta}^k - \dot{\theta}^b$ for $k = 1,\ldots,p$ are the flagella motions in the body frame of reference. Further, $\dot{\theta}^b$, $\dot{z}_x$, and $\dot{z}_y$ are the angular and translational velocities of the cell body, and $\dot{\vartheta}^k$ is the time rate of change of link angles of the $k$th flagellum in the body frame of reference. Matrices $G_{\theta^k}$ and $Q_{\theta^k}$ depend on the flagellum configuration in the inertial frame of reference ($\theta^k$), the fluid drag coefficients, and the distribution of the flagellum on the cell body [$O_1$ in Fig. 2(c)]. These matrices have previously been defined in [30].

The bending moment along the $k$th flagellum that generates the observed motion is given by

$$u^k = B^{-1} \left( N^{\mathrm{T}}_{\theta^k} \Omega^{\mathrm{T}}_{\theta^k} \Gamma \Omega_{\theta^k} N_{\theta^k} \dot{\vartheta}^k + G^{\mathrm{T}}_{\theta^k} \begin{bmatrix} \dot{\theta}^b \\ \dot{z}_x \\ \dot{z}_y \end{bmatrix} \right). \tag{9}$$

Equation (7) shows how the flagella motion is converted into the translational motion of the cell body. Using the observed flagella motion, $\dot{\vartheta}$, we can simulate Eq. (8) to get the translational motion of the body $[\dot{\theta}^b\, \dot{z}_x\, \dot{z}_y]^{\mathrm{T}}$, whereby the thrust is calculated from $f_t$, $f_n$, $c_t$, and $c_n$. We then use Eq. (9) to calculate the bending moment.

In summary, the movement of the cell body resulting from the flagella motion is given by Eq. (8). With this equation, the contributions of $p$ flagella to propulsion can be summed. The thrust along the flagella is then calculated from the velocities of the cell body and flagella using the fluid force model. The relationship between the kinematics of the flagella and the actuation bending moment applied to the flagella is given by Eq. (9).

The actuation bending moment along the $k$th flagellum ($u^k$) and thrust were obtained through simulation of Eqs. (8) and (9), in which the kinematics of the flagella ($\dot{\vartheta}^k$) were constrained to the same motion as the flagella traces collected from the experimental imaging system [26].

## III. RESULTS AND DISCUSSION

### A. Quantitative characterization of flagella kinematics

The kinematics of the flagella was characterized as a traveling wave along the length of the flagellum. The coordinates of the flagella traces for the ventral and anterior flagella [Figs. 2(a) and Figs. 2(b)] were collected using the imaging platform, as described in [26]. The link angle $\theta_i$, where $i \in (0,1)$ is the normalized distance along the flagellum, was measured for each trace [Fig. 2(c)]. The curvature at discrete points $i$ along the flagella was calculated by $\Phi_i(t) := [\theta_{i-\Delta}(t) - \theta_i(t)]/(\Delta l) = \alpha_i \sin(\omega t + \beta_i) + \gamma_i$, where $\Delta$ was the normalized length of the segmental link along the length of the flagella $l$. The amplitude $\alpha_i$, phase $\beta_i$, and bias $\gamma_i$ of curvature variation are shown in Fig. 4. Cumulative phase lag $\beta_i$ [Fig. 4(a)] indicates that a traveling wave proceeds along the ventral flagella, and the curvature of the flagella decreases towards the distal end [Fig. 3(b)]. The bias ($\gamma_i$) characterizes the microscopic shape of the flagellum and the line along which its wave propagates [32]. The average bias ($\gamma_i$) over the flagellum was negative (–4.8 deg/$\mu$m) [Fig. 4(c)], indicating that the cell swims with a slight clockwise turning (zero value of $\gamma_i$ indicates straight swimming) [32]. The kinematics of the anterior flagella was similar to that of the ventral (data not shown).

### B. Forward motion

Planar swimming is driven by the beating of the anterior and ventral flagella, with the ventral flagella constantly beating, and the anterior flagella beating with alternating, simultaneous, or unilateral beating. The posterolateral flagella were not found to participate actively in planar motion, so they were not

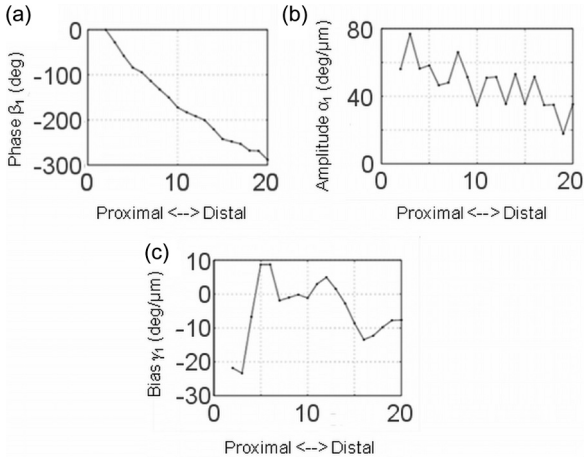


FIG. 4. Analysis of ventral flagella motion. Phase (a), amplitude (b), and bias (c) of the fundamental harmonic of the curvature variation, $\Phi_i(t) = \alpha_i \sin(\omega t + \beta_i) + \gamma_i$, of the ventral flagellum. Cumulative phase lag $\beta_i$ indicates a traveling wave along the flagellum; the curvature of the flagellum decreases towards the distal end. The bias ($\gamma_i$) average over the flagellum is negative (–4.8 deg/$\mu$m), indicating that the cell swims with a slight clockwise turning.

considered in the model. It has been shown in previous studies [37–39] that the synchronized beating of multiple flagella is an energy efficient propulsion mode. In the model, we set the two ventral flagella to beat in phase and the two anterior flagella to beat symmetrically on both sides of the body. The typical length of the ventral flagella and anterior flagella are 7.4 and 5.5 $\mu$m, respectively. Simulations with only anterior flagella beating showed that the cell was propelled forward during the downstroke, and retreated by 58% during the upstroke [30]. However, the constant beating of the ventral flagella generates continuous thrust, whose value varies between the peak value and close to zero during one beating cycle [36,40]. By setting the beating phase of the anterior flagella lagging that of the ventral flagella by 90°, we balanced the drag generated by the upstroke of the anterior flagella with the peak force generated by the ventral flagella, thus eliminating the backward motion, since no retreating motion has been experimentally observed in *Giardia* [26]. The simulated forward swim speed was 7.2 $\mu$m/s. There was a stagnation stage in each beat cycle corresponding with the upstroke of the anterior flagella; however, the coordinated beating of the anterior and ventral flagella prevented any backward motion. Slight backwards motion has been observed in other microorganisms, such as *Chlamydomonas* and *T. foetus*, during the return beat [41–43]. This means that the combination of these flagella results in a more efficient swimming strategy than that of these microorganisms. The results from this analysis confirmed the hypothesis derived from our previous work [30], that the ventral flagella are necessary to prevent an overall backward motion during the beating of the flagella, thus increasing the efficiency of this propulsive strategy.

### C. Actuation bending moment and estimation on motor protein force

The actuation bending moment required to overcome the hydrodynamic resistance for forward motion is shown in Fig. 5(a). The magnitude of the bending moment decreases towards the distal end of the flagellum. The average magnitude of the bending moment at the proximal half portion of the flagellum was 2 pN $\mu$m. To validate the model predictions in the context of known biological data, the model approximations were converted to known measurements. In the model, the length of each link along the flagellum was set to 370 nm, such that the flagellum traces were well approximated by discrete links. The bending moment per unit length was then calculated as 5.4 pN $\mu$m/$\mu$m. This value was comparable to the value obtained from the spermatozoa of the sea urchin *Lytechinus* (5 pN $\mu$m/$\mu$m) [44]. The force generated by a single head of the dynein arms was estimated from the bending moment. Since the spacing between dynein arms along a typical eukaryotic flagellar microtubule is 24 nm [11], and there is an inner and outer dynein arm, each with two heads, we calculated that along each doublet microtubule there were about 62 dynein heads within one link length (370 nm). At present the number of heads present on each dynein arm for *Giardia* is unknown, and limited data exist on the number of dynein proteins in the organism in general [45–47]. However, a recent study conducting genomic analysis of the dyneins present in a wide variety of eukaryotes found that *Giardia*'s outer axonemal dynein arms (OAD) were related to the $\mathrm{OAD}_\beta$ subfamily, which has two heads [45]. Using this genomic analysis, we assume that *Giardia*'s axonemes are two headed, similar to animal axonemes, as opposed to three headed as in some protists, justifying our previous assumption. The cumulative bending moment generated by the relative sliding between doublet microtubules in one half of a flagellum is equivalent to that generated by a single doublet microtubule with the bending arm equal to the diameter of the flagellum (200 nm). From these data, the force per dynein head was calculated as 0.32 pN, which is similar to the value obtained from the spermatozoa of the sea urchin *Lytechinus* (0.35 pN) [44]. The force per dynein head from *Lytechinus* (0.35 pN) was larger than that of *Giardia*; however, the diameter of *Giardia*'s flagellum was 200 nm, compared to the flagella of *Lytechinus*, 160 nm. These predicted forces per dynein head to overcome the hydrodynamic resistance are also consistent with previous reports on the maximal force per dynein arm (with two heads) (1 pN) measured from telescoping flagella [48]. While the data reported from the experimental studies of *Lytechinus* represent the lower bound of reported dynein motor forces [49], the data obtained from this study demonstrate that the model data are within a realistic magnitude. Similarly, the true axoneme structure contains numerous elastic elements,

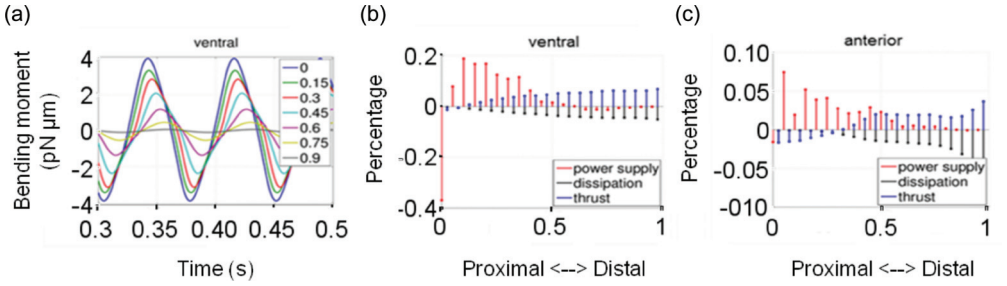


FIG. 5. (Color online) Analysis of bending moment, power supply, and thrust for the ventral and anterior flagella. (a) Predicted actuation bending moment applied at joints along one ventral flagellum. The legend is the normalized distance from the proximal point of the flagellum. (b) and (c) Power supply, dissipation, and thrust distribution along the ventral (b) and anterior (c) flagella. The ventral flagella contribute 64% of the power input and 82% of thrust. The cell body dissipates 8% of the total energy, and the remaining energy is dissipated through the flagella. The total energy supplied in one beating cycle is 598 pN $\mu$m. In both the ventral and anterior flagella, power is mainly supplied at the proximal half portion of the flagellum and dissipated to the fluid continuously along the flagellum. Thrust is positively correlated with the energy dissipation. The majority of thrust is generated from the posterior half portion of the flagellum.

which are expected to generate significant internal drag, and have not been included in the simplified model.

### D. Energy transmission and thrust

The energy supply along the flagella was calculated by the product of the predicted bending moment [Fig. 5(a)] and the time rate of measured curvature change of the flagella (Fig. 4). We found that to achieve the observed planar motion, energy only needs to be supplied at the proximal half portion of the flagellum [Figs. 5(b) and 5(c)]. This energy is dissipated continuously along the flagella with increasing magnitude towards the distal end, with the cell body dissipating about 8% of the total energy. The total energy supplied during one beat was calculated as 598 pN $\mu$m. Thrust was found to be positively correlated with the energy dissipation, such that the more energy released, the more thrust generated [Figs. 5(b) and 5(c)]. It was proposed that the elasticity of the flagella allows for this energy transmission from the proximal to the distal end [36]. In biological systems, the energy necessary to generate the movement of flagella is chemically stored as ATP. Considering the repeating structure of flagella, the flagella can be actuated at any point along its length, assuming that ATP is locally available. Currently, two hypotheses are used to explain the supply of ATP to the flagellar compartment. The first hypothesis states that the ATP necessary for active movement of the flagella is diffused from the cytoplasm to the flagellar compartment, leading to a concentration gradient of ATP along the flagellum, and the narrow aperture and the presence of dense structures at the transition zone plausibly cause the shortage of ATP at the distal region of the flagellum [50]. The second hypothesis states that the flagella contain metabolic enzymes, including flagellum-targeted isoforms of some glycolytic enzymes and adenylate kinases, that allow the generation of ATP from other small metabolic precursors that can be more easily diffused [50]. While these hypotheses are not mutually exclusive, the extent to which each contributes ATP to flagella motion remains unknown. The predictions from our analysis demonstrated that energy provided only at the proximal half portion of the flagellum [Figs. 5(b) and 5(c)] could generate the observed swimming motion, indicating that the most important influx of ATP would be from the cytoplasm, and that a diffuse gradient along the length of the flagella would not affect the motion. While this may be the case for *Giardia*, other eukaryotic cells that have more efficient mechanisms of generating ATP, such as mitochondria, may employ varying degrees of actuation due to different transport mechanisms and a larger pool of available ATP.

### E. Contributions of different pairs of flagella to forward and turning motion

Figures 5(b) and 5(c) illustrated that the ventral flagella contribute 64% of the power input and 82% of the thrust during forward swimming. Experimental analysis found that *Giardia* can readily control its turning angle through beating only one anterior flagellum and that the lateral flexion of the caudal region could lead to a decreased turning radius, as shown in Figs. 6(a) and 6(b). Lateral flexion of the caudal region caused the line, along which the ventral flagella wave propagates, to curve in the same direction as the turning trajectory [Fig. 6(c)] [32]. Such a change in the line along which the flagella wave travels can be regulated by the bias $\gamma_i$ in the curvature function $\alpha_i \sin(\omega t + \beta_i) + \gamma_i$; the larger the bias $\gamma_i$, the larger the curvature of the line along which the flagella wave travels. To analyze the contributions of the anterior and ventral flagella in directional control, three simulations were conducted [Fig. 6(d)]. It was found that the ventral flagella play the major role in regulating the swim direction. For example, by changing the bias $\gamma_i$ in the curvature function $\alpha_i \sin(\omega t + \beta_i) + \gamma_i$ by $\Delta\gamma_i = -7.1$ deg/$\mu$m, *Giardia* can turn at 9° per cycle, and 15° per cycle when the value of $\Delta\gamma_i$ is doubled; meanwhile the turning radius is reduced by 70% [Fig. 5(d), black and blue trajectories]. The beating of one anterior flagellum was able to decrease the turning radius by only 15% [Fig. 5(d), black and red trajectories]. Based on these analyses, we conclude that the ventral flagella generate the majority of the force for turning and forward propulsion during planar swimming. However, the addition of anterior flagella beating to the ventral flagella increased the thrust generated by 18%, and also could minimally alter the turning angle. This simulation shows that the anterior flagella

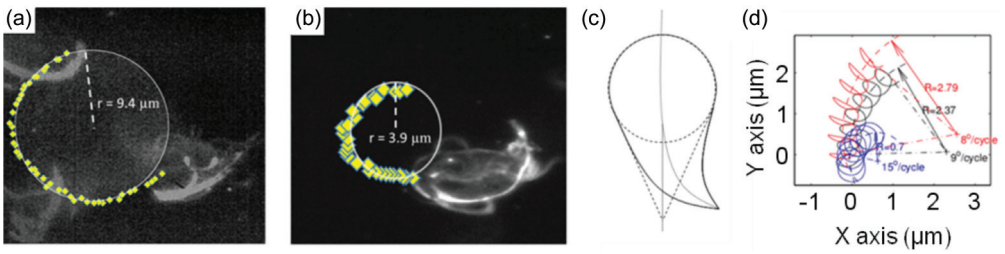


FIG. 6. (Color online) Analysis of turning for *Giardia*. (a) and (b) Plots of turning *Giardia*, with different degrees of lateral flexion of the caudal region. A circle was superimposed on the path for calculation of the turning radius which is 9.4 and 3.9 $\mu$m, respectively. (c) Diagrammatic representation of how *Giardia* is able to change the line along which the wave of ventral flagella propagates by laterally flexing the caudal region. (d) Turning simulations, where the black lines (labeled 9 deg/cycle) show the configuration with the left anterior flagellum beating and the bias of the ventral flagella curvature function $\Phi_i(t) = \alpha_i \sin(\omega t + \beta_i) + \gamma_i$, where $i \in (0,1)$, the normalized distance from the proximal end, equal to $\gamma_i = -7.1°/\mu$m; the red lines (labeled 8 deg/cycle) show without left anterior flagellum beating and $\gamma_i = -7.1$ deg/$\mu$m; the blue lines (labeled 15 deg/cycle) show with the left anterior flagellum beating and $\gamma_i = -14.2$ deg/$\mu$m. The plot demonstrates that regulating the line along which the ventral flagella wave propagates through the bias $\gamma_i$ in the curvature function can effectively tune the turning radius, while the anterior flagella may play a role in fine tuning.

may provide additional, finer control, for planar swimming. Additionally, it has been shown, in attached cells, that the beating of the anterior flagella creates a current past the cell body [26], which may bring nutrients to the cell.

### F. Discussion on bioinspired micropropulsion design for microrobots

One feature of swimming in *Giardia* that can be translated into microrobot design is the actuation of only the proximal portion of the flagella, with the distal portion providing the majority of the propulsive force. For microrobot design, this principle can be considered in the design of a flexible "propeller" with increased surface area on the distal portion to increase the thrust. In addition, instead of actuating the propeller along its entire length, a fixed motor could be attached to the body of the microrobot to drive the propeller.

Another feature that can be translated into microrobot design is the ability to create different beating wave forms, from the same motors. By varying the point of exit of the flagella from the body, the motors can be confined to a central location. Analysis of the anterior and posterolateral flagella revealed that the beating of these flagella was similar to eukaryotic cilia, as opposed to true flagella [Fig. 7(a)]. As indicated in Figs. 7(b) and 7(c), the ciliary beating of the anterior and posterolateral flagella has a significant effect on the direction of fluid motion, and thus propulsion. We expect that the boundary conditions imposed on flagellar beating, both within the cytoplasm and at the point of exit, impart a significant effect in the generation of the observed form. An example of this is the limit on the bending of the flagella imposed by the position of attachment on the body. The flagella could not extend beyond this point, similar to the biomechanical limitation of a hinged joint, such as the knee.

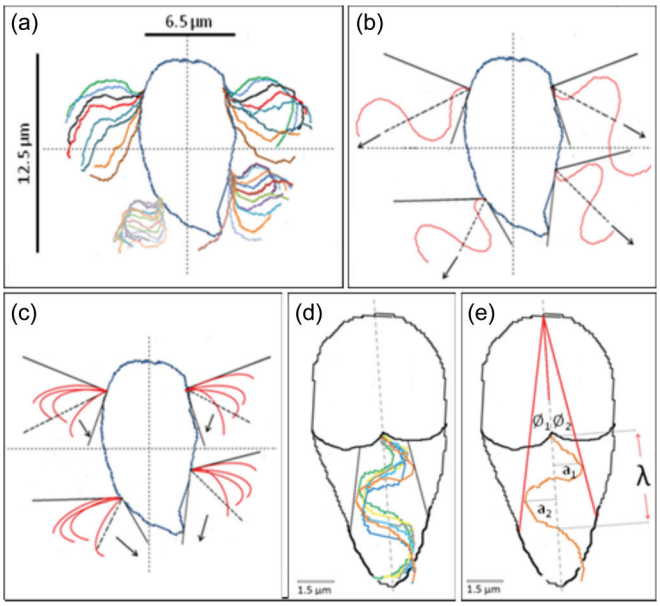


FIG. 7. (Color online) Analysis of plots of anterior, posterolateral, and ventral flagella beating patterns. (a) Note that the traces of the anterior and posterolateral flagella were not sinusoidal. (b) and (c) Fluid motion (arrows) from a sinusoidal (b) or ciliary (c) beating motion. (d) Traces of typical ventral flagella beating over the course of time. Note that the flagella are bounded within the ventrocaudal groove lateral to the flagella. (e) Analysis of a wave generated by the beating of the ventral flagella. The wavelength ($\lambda$) was 3.89 $\mu$m, with a small amplitude crest ($a_1$) of 1.12 $\mu$m originating at the adhesive disc, and a larger amplitude trough ($a_2$) of 1.56 $\mu$m farther down the wave, indicating an expanding wave form. The half angles of the ventrocaudal groove, $\phi_1$ and $\phi_2$, if extended to the midline, were 10.82° and 10.20°.

Unlike the anterior and posterolateral flagella, the ventral flagella emerge at the ventral surface of the cell, parallel to the midline. Analysis of the beating pattern of these flagella indicated that the flagella beat in a true sinusoidal wave form, in stark contrast to the anterior and posterolateral flagella [Fig. 7(d)]. Traces of these flagella over time displayed an undulating symmetrical wave form. Analysis of the motion revealed that the crests and troughs were clearly bounded by the ventrocaudal groove, outlined in Fig. 7(e). Again, the boundary conditions imposed by the cell had a direct effect on the form of the beating motion observed. This principle can be used to design a microrobot using only a single type of motor, but with the body design influencing the movement of the propulsive structures. From an engineering standpoint, the implementation and control of only a single motor type is advantageous and reduces design complexity.

A final component from *Giardia*'s structure that can inspire future microrobot design is the lateral position of the flagella. Previous designs of swimming microrobots have focused mainly on the rearmost placement of bioinspired flagella. While this may be simple, multiflagellated microorganisms have more precise control over their movement by coordinating multiple flagella. In *Giardia*, a combination of laterally placed flagella and posterior-facing flagella provide superior steering and orientation control. As described in Fig. 5, based on the simulation data, the ventral flagella provide the majority of the propulsive force for forward motion; however, the anterior flagella provide fine control over steering and orientation. By studying the movement of the cells, we observed that the alternating beating of the anterior flagella gave the cell more precise control over turning, which would not be possible with only ventral flagella.

## IV. CONCLUSIONS

In this work, RFT [34] was used to model the propulsion of *Giardia* through the generation of planar waves along the flagella. Previous studies have used RFT to model the propulsion of *Giardia* [26,30] and numerous other microorganisms with similar flagella-to-body ratios, such as *Chlamydomonas* [51], although the accuracy of this approach may be improved for multiflagellated swimmers [52,53]. The limitation of RFT is the inability to account for hydrodynamic interactions between flows induced by different pairs of flagella [52]. In the current work, the anterior flagella are positioned on opposite sides of the body, and thus the flows generated by these flagella will not interact, as observed in experimental studies [26]. For the ventral flagella, however, the bounding of these flagella within the ventrocaudal groove is likely to cause the flows generated from each of these flagella to be altered. In addition, since the boundaries of the ventrocaudal groove shape the

wave form of the ventral flagella, the true fluid dynamics within this channel will be highly complex. As recently as 2011, researchers determined that RFT demonstrated good agreement when modeling the cell motion from flagellar forces in a similarly sized microorganism, *Chlamydomonas* [51]. Considering that only ∼35% of the total flagella length during beating is contained within the ventrocaudal groove, with ∼65% extending outside of this boundary with no interference from the cell body, RFT may be used to approximate the fluid motion generated by these flagella.

From the flagella kinematics, we predicted the actuation, mechanical energy supply and dissipation, and thrust along the flagella during planar swimming in *Giardia* using a mechanics model of the flagella-body-fluid interactions. The predicted actuation bending moment and the mechanical energy match the trends observed from the experimental analysis and provide information to support the biological hypotheses, which lend credibility to the model and results. Through mechanics-based analysis of the flagella, we obtained a better understanding of how *Giardia* actuates the flagella and controls propulsion and turning. The findings are summarized as follows: (1) The actuation bending moment along the flagella decreases in magnitude as it approaches the distal end. (2) Energy only needs to be supplied to the proximal half of the flagella. Part of the supplied energy is then transmitted through the elasticity of the flagella to power the passive distal portion. This result demonstrates that a decreasing ATP gradient, from the proximal to distal portion of the flagella, due to the physical constraints imposed in transport of ATP from the cytoplasm to the flagellar compartment, would have no impact on the observed flagellar motion. (3) Energy is dissipated to the fluid continuously along the length of the flagella with increasing magnitude towards the distal end, resulting in the generation of the majority of the thrust at the posterior portion of the flagella. (4) The ventral flagella are the major driving force for propulsion and turning, while the anterior flagella control finer turning motions. These correlations between the propulsive function, ATP gradient, and fine motor control support the hypothesis that the internal mechanisms and structure of biological systems have adapted to generate the swimming gait, which is hypothesized to come from a hydrodynamic optimality. Further study of the motility of microorganisms is crucial to elucidating principles for effective swimming at low Reynold's number, and the diversity of microorganisms and motile strategies provides a great reserve for bioinspiration.

## ACKNOWLEDGMENTS

This research is sponsored by the Office of Naval Research Young Investigator Program award (Grant No. ONR-N00014-11-1-0622) under the supervision of Dr. Thomas McKenna. The authors are grateful for the support.

[1] J. J. Abbott, K. E. Peyer, M. C. Lagomarsino, L. Zhang, L. Dong, I. K. Kaliakatsos, and B. J. Nelson, Int. J. Robot. Res. **28**, 1434 (2009).
[2] M. Sitti, Nature **458**, 1121 (2009).
[3] B. J. Nelson, I. K. Kaliakatsos, and J. J. Abbott, Annu. Rev. Biomed. Eng. **12**, 55 (2010).
[4] G. Kosa, M. Shoham, and M. Zaaroor, IEEE Trans. Robot. **23**, 137 (2007).
[5] J. Edd, S. Payen, B. Rubinsky, M. L. Stoller, and M. Sitti, in *Proceedings of IEEE/RSJ International Conference on Intelligent Robots and Systems, 2003 (IROS 2003)* (IEEE, New York, 2003), pp. 2583–2588.
[6] L. Huaming, T. Jindong, and M. Zhang, IEEE Trans. Autom. Sci. Eng. **6**, 220 (2009).
[7] E. M. Purcell, Am. J. Phys. **45**, 3 (1977).
[8] C. Pozrikidis, *Boundary Integral and Singularity Methods for Linearized Viscous Flow* (Cambridge University Press, Cambridge, 1992).
[9] E. Lauga, Soft Matter **7**, 3060 (2011).
[10] K. H. Bui, G. Pigino, and T. Ishikawa, J. Synchrotron Radiat. **18**, 2 (2011).
[11] L. A. Amos and W. B. Amos, *Molecules of the Cytoskeleton* (Guilford Press, New York, 1991), pp. 253.
[12] I. R. Gibbons, J. Cell Biol. **91**, 107s (1981).
[13] B. Behkam and M. Sitti, J. Dyn. Syst., Meas., Control **128**, 36 (2006).
[14] S. C. Lenaghan, Y. Wang, X. Ning, T. Fukuda, T. Tarn, W. R. Hamel, and M. Zhang, IEEE Trans. Biomed. Eng. **60**, 667 (2013).
[15] A. J. Appelbee, R. C. A. Thompson, and M. E. Olson, Trends Parasitol. **21**, 370 (2005).
[16] P. A. McDonnell, K. G. E. Scott, D. A. Teoh, M. E. Olson, J. A. Upcroft, P. Upcroft, and A. G. Buret, Vet. Parasitol. **111**, 31 (2003).
[17] J. Plutzer and B. Tomor, Parasitol. Int. **58**, 227 (2009).
[18] J. Thompson, R. Yang, M. Power, J. Hufschmid, I. Beveridge, S. Reid, J. Ng, A. Armson, and U. Ryan, Exp. Parasitol. **120**, 88 (2008).
[19] J. A. Upcroft, P. A. McDonnell, and P. Upcroft, Parasitol. Today **14**, 281 (1998).
[20] R. Yang, A. Reid, A. Lymbery, and U. Ryan, Int. J. Parasitol. **40**, 779 (2010).
[21] M. C. Sousa, C. A. Goncalves, V. A. Bairos, and J. Poiares-da-Silva, Clin. Diagn. Lab. Immunol. **8**, 258 (2001).
[22] W. R. Hansen, O. Tulyathan, S. C. Dawson, W. Z. Cande, and D. A. Fletcher, Eukaryotic Cell **5**, 781 (2006).
[23] P. H. Katelaris, A. Naeem, and M. J. Farthing, Gut **37**, 512 (1995).
[24] E. A. Meyer, Exp. Parasitol. **39**, 101 (1976).
[25] W. K. Seow, A. A. Crouch, and Y. H. Thong, Trans. R. Soc. Trop. Med. Hyg. **79**, 359 (1985).
[26] S. C. Lenaghan, C. A. Davis, W. R. Henson, Z. Zhang, and M. Zhang, Proc. Natl. Acad. Sci. USA **108**, E550 (2011).
[27] H. G. Elmendorf, S. C. Dawson, and J. M. McCaffery, Int. J. Parasitol. **33**, 3 (2003).
[28] D. V. Holberton, J. Exp. Biol. **60**, 207 (1974).
[29] D. Tam and A. E. Hosoi, Proc. Natl. Acad. Sci. USA **108**, 1001 (2011).

[30] J. Chen, S. C. Lenaghan, and M. Zhang, in *Proceedings of IEEE International Conference on Robotics and Automation (ICRA)* (IEEE, New York, 2012), pp. 4204–4209.
[31] C. P. Lowe, Philos. Trans. R. Soc., B **358**, 1543 (2003).
[32] M. Saito, M. Fukaya, and T. Iwasaki, IEEE Control Syst. Mag. **22**, 64 (2002).
[33] C. J. Brokaw, Biol. J. Linn. Soc. **7** (Suppl. 1), 423 (1975).
[34] J. Gray and G. J. Hancock, J. Exp. Biol. **32**, 802 (1955).
[35] J. Happel and H. Brenner, *Low Reynolds Number Hydrodynamics: With Special Applications to Particulate Media* (Springer, New York, 1965), Vol. 1.
[36] J. Chen, W. O. Friesen, and T. Iwasaki, J. Exp. Biol. **214**, 561 (2011).
[37] G. Taylor, Proc. R. Soc. London, Ser. A **209**, 447 (1951).
[38] R. Golestanian, J. M. Yeomans, and N. Uchida, Soft Matter **7**, 3074 (2011).
[39] Y. Z. Yang, J. Elgeti, and G. Gompper, Phys. Rev. E **78**, 061903 (2008).
[40] I. Borazjani and F. Sotiropoulos, J. Exp. Biol. **212**, 576 (2009).
[41] C. J. Brokaw and D. J. L. Luck, Cell Motil. **3**, 131 (1983).
[42] L. H. Monteiro-Leal, M. Farina, M. Benchimol, B. Kachar, and W. De Souza, J. Eukaryotic Microbiol. **42**, 709 (1995).
[43] L. H. Monteiro-Leal, M. Farina, and W. de Souza, Cell Motil. Cytoskeleton **34**, 206 (1996).
[44] C. J. Brokaw, in *Molecules and Cell Movement*, edited by S. Inoue and R. E. Stephens (Raven Press, New York, 1975), pp. 165.
[45] B. Wickstead and K. Gull, Traffic **8**, 1708 (2007).
[46] S. W. Roy, A. J. Hudson, J. Joseph, J. Yee, and A. G. Russell, Mol. Biol. Evol. **29**, 43 (2012).
[47] S. C. Dawson, in *Giardia: A Model Organism*, edited by H. D. Luján and S. Svärd (Springer, Vienna, 2011), pp. 400.
[48] S. Kamimura and K. Takahashi, Nature **293**, 566 (1981).
[49] A. K. Rai, A. Rai, A. J. Ramaiya, R. Jha, and R. Mallik, Cell **152**, 172 (2013).
[50] M. L. Ginger, N. Portman, and P. G. McKean, Nat. Rev. Microbiol. **6**, 838 (2008).
[51] P. V. Bayly, B. L. Lewis, E. C. Ranz, R. J. Okamoto, R. B. Pless, and S. K. Dutcher, Biophys. J. **100**, 2716 (2011).
[52] B. Rodenborn, C.-H. Chen, H. L. Swinney, B. Liu, and H. P. Zhang, Proc. Natl. Acad. Sci. USA **110**, E338 (2013).
[53] E. Lauga and T. R. Powers, Rep. Prog. Phys. **72**, 096601 (2009).